J|A|C|S ARTICLES

Published on Web 04/09/2009

Observation of Redox-Induced Electron Transfer and Spin Crossover for Dinuclear Cobalt and Iron Complexes with the 2,5-Di-*tert*-butyl-3,6-dihydroxy-1,4-benzoquinonate Bridging Ligand

Kil Sik Min,[†,‡] Antonio G. DiPasquale,[§] Arnold L. Rheingold,[§] Henry S. White,[†] and Joel S. Miller*[,†]

Department of Chemistry, University of Utah, Salt Lake City, Utah 84112-0850, Department of Chemistry Education, Kyungpook National University, Daegu 702-701, Republic of Korea, and Department of Chemistry, University of California, San Diego, La Jolla, California 92093-0358

Received February 5, 2009; E-mail: jsmiller@chem.utah.edu

Abstract: Dinuclear $[(TPyA)M^{II}(DBQ^{2-})M^{II}(TPyA)](BF_4)_2$ [TPyA = tris(2-pyridylmethyl)amine; DBQ^{2-} = 2,5-di-*tert*-butyl-3,6-dihydroxy-1,4-benzoquinonate; M = Co (**1**$^{2+}$), Fe (**2**$^{2+}$), Ni (**3**$^{2+}$)] complexes have been prepared by the reaction of M^{2+}, TPyA, H_2DBQ, and triethylamine in MeOH solution. Their monooxidized form $[(TPyA)M^{III}(DBQ^{\bullet 3-})M^{III}(TPyA)]^{3+}$ [Co = (**1**$^{3+}$), Fe (**2**$^{3+}$)] has been synthesized by using ferrocenium tetrafluoroborate, and the dioxidized form of **1**$^{2+}$, $[(TPyA)Co^{III}(DBQ^{2-})Co^{III}(TPyA)]^{4+}$ (**1**$^{4+}$), has been obtained by using thianthrinium tetrafluoroborate. These dinuclear compounds were characterized by X-ray crystallography, electrochemistry, magnetism, and EPR spectroscopy. Valence ambiguous **1**$^{3+}$ forms via redox-induced electron transfer, whereby the one-electron oxidation of the $[Co^{II}(DBQ^{2-})Co^{II}]^{2+}$ core forms $[Co^{III}(DBQ^{\bullet 3-})Co^{II}]^{3+}$, and it also exhibits spin crossover behavior to the core $[Co^{III}(DBQ^{2-})Co^{II}]^{3+}$ above room temperature. The M ions in **1** and **2** have a distorted octahedral geometry by coordination with four nitrogens of a TPyA, two oxygens of a $DBQ^{2-/\bullet 3-}$. Due to the interdimer offset face-to-face $\pi-\pi$ and/or herringbone interactions, **1**$^{2+}$, **1**$^{3+}$, and **2**$^{2+}$ show extended 1-D and/or 2-D supramolecular structures. The existence of $DBQ^{\bullet 3-}$ in **1**$^{3+}$ is confirmed from both solid-state magnetic and solution EPR data. Co- and Ni-based **1**$^{2+}$ and **3**$^{2+}$ show weak antiferromagnetic interactions [**1**$^{2+}$: $g = 2.44$, $J/k_B = -3.20$ K (-2.22 cm^{-1}); **3**$^{2+}$: $g = 2.13$, $J/k_B = -3.22$ K (-2.24 cm^{-1}), $H = -2J\mathbf{S}_1\cdot\mathbf{S}_2$ for **1**$^{2+}$ and **3**$^{2+}$], while Fe-based **2**$^{2+}$ exhibits strong spin crossover behavior above room temperature. **1**$^{2+}$ has three reversible one-electron transfer waves at $E_{1/2}$ (vs SCE in MeCN) = -1.121, 0.007, and 0.329 V, and a fourth wave at -1.741 V that exhibits a slight chemical irreversibility. The first three correspond to $[Co^{II}DBQ^{2-}Co^{II}]^{2+}$ reduction to $[Co^{II}DBQ^{\bullet 3-}Co^{II}]^{+}$, and oxidation to $[Co^{III}DBQ^{\bullet 3-}Co^{II}]^{3+}$ and $[Co^{III}DBQ^{2-}Co^{III}]^{4+}$, respectively. The mechanism of the multielectron transfer oxidation from $[Co^{II}DBQ^{2-}Co^{II}]^{2+}$ to $[Co^{III}DBQ^{\bullet 3-}Co^{III}]^{3+}$ is unknown; the energy of stabilization for oxidizing the Co^{II} centers in the presence of $DBQ^{\bullet 3-}$, relative to oxidizing the Co^{II} centers in the presence of DBQ^{2-} is computed to be 1.45 eV. **2**$^{2+}$ also has three reversible one-electron transfer waves at 0.802, 0.281, and -1.007 V that correspond to two successive one-electron oxidations (**2**$^{2+}$/**2**$^{3+}$ and **2**$^{3+}$/**2**$^{4+}$), and a one-electron reduction (**2**$^{2+}$/**2**$^{+}$). **2**$^{2+}$ has the $[Fe_{hs}^{II}(DBQ^{2-})Fe_{hs}^{II}]^{2+}$ electronic structure that becomes $[Fe_{hs}^{III}(DBQ^{\bullet 3-})Fe_{hs}^{III}]^{3+}$ upon oxidation. The latter undergoes spin crossover above room temperature to populate the $[Fe_{hs}^{III}(DBQ^{2-})Fe_{hs}^{II}]^{3+}$ excited state.

Introduction

Dinuclear metal complexes have attracted considerable interest due to the structural elucidation of metalloenzymes and redox catalysts, as well as the mechanistic understanding of spin-coupled systems.[1] Recently, dinuclear cobalt and iron complexes bridged with chloranilate $(CA^{2-/\bullet 3-})$[2] and related tetraoxolate[3] having a delocalized π system have been shown to exist in different oxidation states. The Co-based $[(TPyA)Co^{II}(CA^{2-})Co^{II}(TPyA)](BF_4)_2$ complex shows weak antiferromagnetic interactions, while Fe-based $[(TPyA)Fe^{II}(CA^{2-})Fe^{II}(TPyA)](BF_4)_2$ exhibits weak ferromagnetic interactions. In addition, the species with $CA^{\bullet 3-}$ present in cobalt and iron dinuclear complexes exhibit much stronger spin coupling than those with CA^{2-}, due to direct spin coupling to the radical. Furthermore, the formation of $CA^{\bullet 3-}$ in $[(TPyA)Co^{III}(CA^{\bullet 3-})Co^{III}(TPyA)](BF_4)_3$ occurred via a redox-induced electron transfer (RIET) reaction,[4] in which addition of 1 equiv of an oxidant results in the oxidation of two metal centers and reduction of the CA^{2-} bridging ligand.[5] In contrast, the iron(II) dinuclear complex bridged with DBQ^{2-} (DBQ^{2-} = 2,5-di-*tert*-butyl-3,6-dihydroxy-

† University of Utah.
‡ Kyungpook National University.
§ University of California, San Diego.

(1) (a) Williams, N. H.; Cheung, W.; Chin, J. *J. Am. Chem. Soc.* **1998**, *120*, 8079. (b) Tshuva, E. Y.; Lippard, S. J. *Chem. Rev.* **2004**, *104*, 987. (c) Wada, T.; Tsuge, K.; Tanaka, K. *Inorg. Chem.* **2001**, *40*, 329. (d) Zilbermann, I.; Maimon, E.; Cohen, H.; Meyerstein, D. *Chem. Rev.* **2005**, *105*, 2609. (e) Poulsen, A. K.; Rompel, A.; McKenzie, C. J. *Angew. Chem., Int. Ed.* **2005**, *44*, 6916. (f) Hicks, R. G.; Lemaire, M. T.; Thompson, L. K.; Barclay, T. M. *J. Am. Chem. Soc.* **2000**, *122*, 8077. (g) Benelli, C.; Gatteschi, D. *Chem. Rev.* **2002**, *102*, 2369.

Chart 1

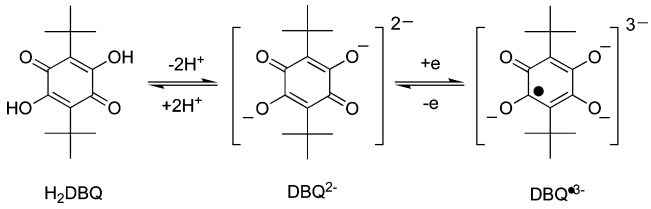

1,4-benzoquinonate), i.e., $[(TPyA)Fe^{II}(DBQ^{2-})Fe^{II}(TPyA)](BF_4)_2$, exhibits spin crossover behavior around room temperature.[6] In addition, the iron(II) dinuclear complex bridged with $THBQ^{2-}$ ($THBQ^{2-}$ = 2,3,5,6-tetrahydroxy-1,4-benzoquinonate), i.e., $[(TPyA)Fe^{II}(THBQ^{2-})Fe^{II}(TPyA)](BF_4)_2$, also exhibits spin crossover ~250 K, with a 10 K hysteresis, and displays ferromagnetic coupling between the iron(II) ions.[7] From these iron(II) dinuclear complexes, we recognized that the magnetic behaviors are very sensitive to the substituent on the bridging anilate ligand. To explore this chemistry the more electron donating *tert*-butyl group, i.e., DBQ^{2-} (Chart 1) was targeted to explore its affect on the magnetic properties, e.g., spin coupling and spin crossover, and herein on the formation and characterization of a series of isostructural dicobalt, diiron, and dinickel complexes bridged by 2,5-di-*tert*-butyl-3,6-dihydroxy-1,4-benzoquinonate (DBQ^{2-} or $DBQ^{\bullet 3-}$) is reported. In particular, we observed that Co-based dinuclear complex with $DBQ^{\bullet 3-}$ shows valence-tautomeric spin crossover behavior above room temperature, while Fe-based complexes exhibit spin crossover behavior. Note that this redox reaction in the cobalt complex can be described as a RIET, whereby the one-electron oxidation of the $[Co^{II}DBQ^{2-}Co^{II}]^{2+}$ core forms $[Co^{III}DBQ^{\bullet 3-}Co^{III}]^{3+}$, not the expected mixed-valent $[Co^{II}DBQ^{2-}Co^{III}]^{3+}$ core. DBQ^{2-} is expected to provide a weak spin interaction, as occurs for CA^{2-}. While both cobalt and nickel form dinuclear complexes with DBQ^{2-} and exhibit weak magnetic interactions, only the iron dinuclear complex unexpectedly displays spin crossover behavior.

Experimental Section

All chemicals used in the synthesis were of reagent grade and used without further purification. Tris(2-pyridylmethyl)amine (TPyA),[8a] $[Ni(MeCN)_6](BF_4)_2$,[8b] and thianthrinium tetrafluoroborate ($ThianBF_4$)[8c] were prepared according to literature procedures. Ferrocenium tetrafluoroborate ($FcBF_4$) and 2,5-di-*tert*-butyl-3,6-dihydroxy-1,4-benzoquinone (H_2DBQ) were used as received from Aldrich and Interbioscreen Ltd., respectively. Solvents were distilled from the appropriate drying agents under nitrogen before use. All syntheses were performed in a wet or dry oxygen-free (<1 ppm O_2) box. Infrared spectra were recorded with a Bruker Tensor 37 FT-IR spectrophotometer (±1 cm^{-1}). Cyclic voltammograms (CVs) were obtained using an EPSILON electrochemistry analyzer in MeCN [0.1 M $[N(n\text{-}Bu)_4]BF_4$ supporting electrolyte] at a scan rate 100 mV s^{-1} using a Pt working electrode vs a saturated calomel electrode (SCE). Ferrocenium/ferrocene (Fc^+/Fc) was used to calibrate the SCE, and the data are reported vs the SCE. Elemental analyses were performed by Chemisar Laboratories. Magnetic susceptibilities were measured in applied fields of 1, 3, 5, and 10 kOe between 2 and 300 or 380 K on a Quantum Design MPMS superconducting quantum interference device (SQUID) magnetometer as previously reported.[9] Diamagnetic corrections [586 ($\mathbf{1}^{2+}$), 619 ($\mathbf{1}^{3+}$), 588 ($\mathbf{2}^{2+}$), 615 ($\mathbf{2}^{3+}$) and 604 × 10^{-6} ($\mathbf{3}^{2+}$) emu/mol] were made by using Pascal's constants. X-band EPR spectra were recorded on a Bruker EMX-EPR spectrometer.

$[(TPyA)Co^{II}(DBQ^{2-})Co^{II}(TPyA)](BF_4)_2$ ($\mathbf{1}^{2+}$). To a 10-mL MeOH solution of $Co(BF_4)_2 \cdot 6H_2O$ (137 mg, 0.40 mmol) was added a MeOH solution (10 mL) of TPyA (117 mg, 0.40 mmol) and a MeOH solution (10 mL) of H_2DBQ (50 mg, 0.20 mmol) in a wet box (<1 ppm O_2), and the solution became dark red-brown. Triethylamine (0.06 mL, 0.40 mmol) was added to the mixture for neutralization, upon which the solution became red-brown, and subsequently heated to reflux for 30 min. After cooling to room temperature, the solution was filtrated and then concentrated to ~1/4 of the original volume and allowed to stand in a refrigerator for 1 day, and dark red-brown crystals formed were collected by filtration and washed with methanol, and dried in vacuo [Yield: 140 mg (62%)]. Anal. Calcd for $C_{50}H_{54}B_2Co_2F_8N_8O_4$: C, 53.50; H, 4.85; N, 9.98. Found: C, 53.84; H, 5.09; N, 9.99. FT-IR (KBr): ν_{CH} 3081 (w), 2949 (m), 1606 (s), ν_{CO} 1496 (vs), 1447 (s), 1344 (s), 1290 (m), 1059 (multiple, br), 904 (w), 764 (s) cm^{-1}.

$[(TPyA)Co^{III}(DBQ^{\bullet 3-})Co^{III}(TPyA)](BF_4)_3$ ($\mathbf{1}^{3+}$). In a drybox a 2.0-mL MeCN solution of $\mathbf{1}^{2+}$ (38 mg, 0.034 mmol) was added to 2.0 mL MeCN solution of $FcBF_4$ (9.2 mg, 0.034 mmol), the color became dark red, and the solution was stirred for 30 min at room temperature. Dark red block-shaped crystals of $\mathbf{1}^{3+}$ were obtained by diffusion of diethyl ether into the reaction mixture of acetonitrile for 2 or 3 days and were collected by filtration and washed with MeCN and dried in vacuo [Yield: 31 mg (76%)]. Anal. Calcd for $C_{50}H_{54}B_3Co_2F_{12}N_8O_4$: C, 49.66; H, 4.50; N, 9.27. Found: C, 48.92; H, 4.96; N, 9.06 FT-IR (KBr): ν_{CH} 3117 (w), 2972 (m), 1611 (s), ν_{CO} 1516 (s), 1487 (s), 1447 (s), 1375 (vs), 1288 (s), 1060 (multiple, br), 906 (m), 769 (s) cm^{-1}.

$[(TPyA)Co^{III}(DBQ^{2-})Co^{III}(TPyA)](BF_4)_4$ ($\mathbf{1}^{4+}$). In a drybox a 4.0-mL MeCN solution of $\mathbf{1}^{2+}$ (35 mg, 0.031 mmol) was added an MeCN solution (3 mL) of $ThianBF_4$ (19 mg, 0.062 mmol), the color became yellow-brown, and the solution was stirred for 1 h at room temperature. Yellow-brown block-shaped crystals of $\mathbf{1}^{4+}$ were obtained by diffusion of diethyl ether into the reaction mixture of acetonitrile for 2 or 3 days, and were collected by filtration and washed with MeCN and dried in vacuo [Yield: 30 mg (74%)]. Anal. Calcd for $C_{50}H_{54}B_4Co_2F_{16}N_8O_4$: C, 46.33; H, 4.20; N, 8.65. Found: C, 45.91; H, 4.16; N, 9.02. FT-IR (KBr): ν_{CH} 3125 (w), 2973 (m), 1613 (s), ν_{CO} 1481 (vs), 1453 (s), 1333 (s), 1288 (s), 1057 (multiple, br), 770 (s), 521 (m) cm^{-1}.

$[(TPyA)Fe^{II}(DBQ^{2-})Fe^{II}(TPyA)](BF_4)_2$ ($\mathbf{2}^{2+}$). In a wet box a 50-mL MeOH solution of $Fe(BF_4)_2 \cdot 6H_2O$ (232 mg, 0.688 mmol) was added a 10-mL MeOH solution of TPyA (200 mg, 0.688 mmol) and a MeOH solution (10 mL) of H_2DBQ (87 mg, 0.344 mmol), and the color became dark green. Triethylamine (0.10 mL, 0.688 mmol) was added to the mixture for neutralization, and the solution became dark green, and was stirred for 1 h at room temperature. After filtration, the solution was concentrated to ~1/3 of the original

(2) (a) Kitagawa, S.; Kawata, S. *Coord. Chem. Rev.* **2002**, *224*, 11. (b) Min, K. S.; Rheingold, A. L.; DiPasquale, A.; Miller, J. S. *Inorg. Chem.* **2006**, *45*, 6135.
(3) (a) Dei, A.; Gatteschi, D.; Pardi, L.; Russo, U. *Inorg. Chem.* **1991**, *30*, 2589. (b) Tao, J.; Maruyama, H.; Sato, O. *J. Am. Chem. Soc.* **2006**, *128*, 1790. (c) Carbonera, C.; Dei, A.; Létard, J.-F.; Sangregorio, C.; Sorace, L. *Agnew. Chem., Int. Ed.* **2004**, *43*, 3136. (d) Li, B.; Tao, J.; Sun, H.-L.; Sato, O.; Huang, R.-B.; Zheng, L.-S. *Chem. Commun.* **2008**, 2269. (e) Sato, O.; Miura, S.; Maruyama, H.; Zhang, Y.; Wu, D.; Zhang, W.; Xu, H.; Matsuda, R.; Sun, H.; Tao, J. *Inorg. Chim. Acta* **2008**, *361*, 3659.
(4) Miller, J. S.; Min, K. S. *Angew. Chem., Int. Ed.* **2009**, *48*, 262. *Angew. Chem.* 2009, *121*, 268.
(5) Min, K. S.; DiPasquale, A. G.; Golen, J. A.; Rheingold, A. L.; Miller, J. S. *J. Am. Chem. Soc.* **2007**, *129*, 2360.
(6) Min, K. S.; DiPasquale, A.; Rheingold, A. L.; Miller, J. S. *Inorg. Chem.* **2007**, *46*, 1048.
(7) Min, K. S.; Swierczek, K.; DiPasquale, A. G.; Rheingold, A. L.; Reiff, W. M.; Arif, A. M.; Miller, J. S. *Chem. Commun.* **2008**, 317.
(8) (a) Tyeklár, Z.; Jacobson, R. R.; Wei, N.; Murthy, N. N.; Zubieta, J.; Karlin, K. D. *J. Am. Chem. Soc.* **1993**, *115*, 2677. (b) Heintz, R. A.; Smith, J. A.; Szalay, P. S.; Weisgerber, A.; Dunbar, K. R.; Beck, K.; Coucouvanis, D. *Inorg. Synth.* **2002**, *33*, 75. (c) Boduszek, B.; Shine, H. J. *J. Org. Chem.* **1988**, *53*, 5142.
(9) Brandon, E. J.; Rittenberg, D. K.; Arif, A. M.; Miller, J. S. *Inorg. Chem.* **1998**, *37*, 3376.

Table 1. Summary of the Crystallographic Data for $\mathbf{1}^{n+}$ (n = 2, 3, 4) and $\mathbf{2}^{2+}$

	$\mathbf{1}^{2+}$	$\mathbf{1}^{3+}$	$\mathbf{1}^{4+}$	$\mathbf{2}^{2+c}$	$\mathbf{2}^{2+d}$
formula	$C_{51}H_{58}B_2Co_2F_8N_8O_5$	$C_{54}H_{60}B_3Co_2F_{12}N_{10}O_4$	$C_{56}H_{63}B_4Co_2F_{16}N_{14}O_4$	$C_{50}H_{54}B_2F_8Fe_2N_8O_4$	$C_{50}H_{54}B_2F_8Fe_2N_8O_4$
M_r	1154.53	1291.41	1461.30	1116.33	1116.33
crystal system	monoclinic	monoclinic	monoclinic	monoclinic	monoclinic
space group	$P2_1/c$	$C2/c$	$P2_1/n$	$P2_1/c$	$P2_1/c$
a (Å)	15.308(1)	24.120(2)	17.953(3)	15.245(2)	15.398(2)
b (Å)	17.834(1)	15.404(1)	19.739(3)	18.481(3)	18.553(2)
c (Å)	20.326(2)	17.058(1)	19.190(3)	19.241(3)	19.548(2)
α (deg)	90	90	90	90	90
β (deg)	108.407(1)	116.964(1)	109.888(2)	107.588(2)	107.824(2)
γ (deg)	90	90	90	90	90
V (Å^3)	5265.0(7)	5648.9(8)	6394.9(16)	5167.4(14)	5316.4(9)
Z	4	4	4	4	4
D_{calc} (g cm^{-3})	1.457	1.518	1.518	1.435	1.395
T (K)	100(2)	208(2)	100(2)	208(2)	298(2)
μ Mo Kα (mm^{-1})	0.713	0.683	0.623	0.643	0.625
R1[a] (4σ data)	0.0480	0.0550	0.0778	0.0864	0.0598
wR2[b] (4σ data)	0.1274	0.1375	0.1916	0.2438	0.1782

[a] $R1 = \Sigma||F_o| - |F_c||/\Sigma|F_o|$. [b] $wR2 = [\Sigma w(F_o^2 - F_c^2)^2/\Sigma w(F_o^2)^2]^{1/2}$. [c] 208(2) K.[6] [d] 298(2) K.[6]

volume and allowed to stand in a refrigerator for 2 or 3 days, and dark brown crystals formed that were collected by filtration and washed with methanol, and dried in vacuo [Yield: 200 mg (52%)]. Anal. Calcd for $C_{50}H_{54}B_2F_8Fe_2N_8O_4$: C, 53.80; H, 4.88; N, 10.04. Found: C, 54.11; H, 5.04; N, 10.19. FT-IR (KBr): ν_{CH} 3078 (w), 2951 (m), 1605 (s), 1573 (w), ν_{CO} 1502 (vs), 1485 (sh, vs), 1442 (vs), 1335 (s), 1160 (m), 1055 (multiple, br), 905 (m), 763 (s), 655 (m), 521 (m) cm^{-1}.

[(TPyA)Fe^{III}(DBQ$^{\bullet 3-}$)Fe^{III}(TPyA)](BF$_4$)$_3$ ($\mathbf{2}^{3+}$). In a drybox a 10-mL CH_2Cl_2 solution of $\mathbf{2}^{2+}$ (138 mg, 0.124 mmol) was added a CH_2Cl_2 solution (10 mL) of $FcBF_4$ (34 mg, 0.124 mmol), the color became dark brown, and the solution was stirred for 1 h at room temperature. Dark green plate-shaped crystals of $\mathbf{2}^{3+}$ were obtained during the stirring, and were collected by filtration and washed with CH_2Cl_2 and dried in vacuo [Yield: 135 mg (91%)]. Anal. Calcd for $C_{50}H_{54}B_3F_{12}Fe_2N_8O_4$: C, 49.91; H, 4.52; N, 9.31. Found: C, 49.95; H, 4.72; N, 9.09. FT-IR (KBr): ν_{CH} 3113 (w), 2957 (m), 1609 (s), ν_{CO} 1486 (s), 1446 (s), 1316 (s), 1055 (multiple, vs), 903 (m), 771 (s), 521 (m) cm^{-1}.

[(TPyA)Ni^{II}(DBQ^{2-})Ni^{II}(TPyA)](BF$_4$)$_2$ ($\mathbf{3}^{2+}$). In a wet box a 4-mL MeOH solution of $[Ni(MeCN)_6](BF_4)_2$ (151 mg, 0.315 mmol) was added a 4-mL MeOH solution of TPyA (92 mg, 0.315 mmol) and a MeOH solution (4 mL) of H_2DBQ (39 mg, 0.155 mmol), and the color became red. Triethylamine (0.05 mL, 0.344 mmol) was added to the mixture for neutralization, and the solution became red, and was stirred for 2 h at room temperature. Red crystals formed that were collected by filtration and washed with methanol, and dried in vacuo [Yield: 135 mg (76%)]. Anal. Calcd for $C_{50}H_{54}B_2F_8N_8Ni_2O_4$: C, 53.52; H, 4.85; N, 9.99. Found: C, 53.76; H, 5.12; N, 9.85. FT-IR (KBr): ν_{CH} 3058 (w), 2950 (m), 1605 (s), ν_{CO} 1496 (vs), 1447 (s), 1347 (s), 1052 (multiple, br), 904 (w), 764 (m), 645 (w) cm^{-1}.

X-ray Crystallographic Data Collection and Refinement. Dark red-brown crystals of $\mathbf{1}^{2+}$, dark red crystals of $\mathbf{1}^{3+}$, and yellow-brown crystals of $\mathbf{1}^{4+}$ were mounted on a CryoLoop with Paratone oil. Intensity data for all structures were collected with a Bruker APEX CCD detector, and the data were integrated using the Bruker SAINT software program.[10a,b] The intensity data were corrected for absorption using the SADABS program with multiscan data.[10c] The structures were solved by direct ($\mathbf{1}^{2+}$, $\mathbf{1}^{4+}$)[11a] or Patterson methods ($\mathbf{1}^{3+}$)[11b] and refined by full-matrix least-squares methods using SHELXL-97.[11c] The positions of all non-hydrogen atoms were refined with anisotropic displacement factors. All hydrogen atoms were placed using a riding model, and their positions were constrained relative to their parent atom using the appropriate HFIX command in SHELXL-97, except the hydrogens of MeCN in $\mathbf{1}^{3+}$. Due to the disorder, the four BF_4^- anions per unit cell for $\mathbf{1}^{3+}$ (one of three BF_4^- anions per $\mathbf{1}^{3+}$ was treated with the SQUEEZE), and all MeCN molecules and BF_4^- anions of $\mathbf{1}^{4+}$ were treated with the SQUEEZE routine in the program PLATON[11d] and were omitted from the final refinements as atomic contributions, but are included in the computation of intensive properties. The crystallographic data of $\mathbf{1}^{2+}$, $\mathbf{1}^{3+}$, and $\mathbf{1}^{4+}$, including $\mathbf{2}^{2+}$ at 208 and 298 K, are summarized in Table 1.

Results and Discussion

Synthesis and Characterization. The reaction of 1 equiv of TPyA and 0.5 equiv of H_2DBQ with $M(BF_4)_2 \cdot 6H_2O$ (M = Co, Fe) or $[Ni(MeCN)_6](BF_4)_2$ in MeOH solution containing 1 equiv of triethylamine under a nitrogen atmosphere in a wet box affords the dinuclear complexes, [(TPyA)Co(DBQ)Co(TPyA)]-$(BF_4)_2$ ($\mathbf{1}^{2+}$, dark red-brown), [(TPyA)Fe(DBQ)Fe(TPyA)]$(BF_4)_2$ ($\mathbf{2}^{2+}$, dark brown), and [(TPyA)Ni(DBQ)Ni(TPyA)]$(BF_4)_2$ ($\mathbf{3}^{2+}$, red) in good yield, respectively. In accord with the cyclic voltammetry (vide infra), $\mathbf{1}^{3+}$ and $\mathbf{1}^{4+}$ were respectively prepared from the oxidation with 1 equiv of $FcBF_4$ and 2 equiv of thianthrinium tetrafluoroborate (Thian$^+$/Thain, 1.23 V vs SCE)[12] at room temperature in a drybox, respectively. Dark red and yellow brown crystals of valence ambiguous [(TPyA)Co(DBQ)-Co(TPyA)]$^{3+}$ ($\mathbf{1}^{3+}$) and fully oxidized [(TPyA)Co(DBQ)-Co(TPyA)]$^{4+}$ ($\mathbf{1}^{4+}$) were obtained in 76% and 74% yields, respectively. Dark green, solvent-sensitive crystals [(TPyA)Fe-(DBQ)Fe(TPyA)]$(BF_4)_3$ ($\mathbf{2}^{3+}$) were obtained in 91% yield via $FcBF_4$ oxidation of $\mathbf{2}^{2+}$.

Attempts to obtain $\mathbf{3}^+$ from $\mathbf{3}^{2+}$ failed due to the decomposition of the dimer during the reduction process. The structures and electronic structures of $\mathbf{1}^{n+}$ (n = 2, 3, 4), $\mathbf{2}^{n+}$ (n = 2,[6] 3), and $\mathbf{3}^{2+}$ were elucidated from the elemental analysis, infrared spectrum, electrochemistry, solution EPR, solid-state magnetochemistry, and single crystal X-ray diffraction analysis. $\mathbf{3}^{2+}$ exhibits the same IR spectrum as $\mathbf{1}^{2+}$ or $\mathbf{2}^{2+}$, thus, it is assigned

(10) (a) *Saint Plus, v. 6.02*; Bruker Analytical X-ray: Madison, WI, 1999. (b) Sheldrick G. M. *SADABS*; University of Göttingen: Göttingen, Germany, 1996. (c) Sheldrick G. M. *SADABS*; University of Göttingen: Göttingen, Germany, 1996.

(11) (a) Burla, M. C.; Caliandro, R.; Camalli, M.; Carrozzini, B.; Cascarano, G. L.; De Caro, L.; Giacovazzo, C.; Polidori, G.; Spagna, R. SIR2004. (b) Beurskens, P. T.; Beurskens, G.; de Gelder, R.; Garcia-Granda, S.; Gould, R. O.; Israel, R.; Smits, J. M. M. *The DIRDIF-99 program system*; Crystallography Laboratory, University of Nijmegen: Nijmegen, The Netherlands, 1999. (c) SheldrickG. M. *SHELXL97, program for the crystal structure refinement*; University of Göttingen: Göttingen, Germany, 1997. (d) Spek, A. L. *J. Appl. Crystallogr.* **2003**, *36*, 7.

(12) Connelly, N. G.; Geiger, W. E. *Chem. Rev.* **1996**, *96*, 877.

Table 2. Selected Bond Distances (Å) for $\mathbf{1}^{n+}$ (n = 2, 3, 4) and $\mathbf{2}^{2+}$

	$\mathbf{1}^{2+}$	$\mathbf{1}^{3+}$	$\mathbf{1}^{4+}$	$\mathbf{2}^{2+a}$	$\mathbf{2}^{2+b}$
M1−M2	7.820(1)	7.488(2)	7.499(1)	7.616(1)	7.663(2)
M1−N1	2.157(2)	1.942(2)	1.952(4)	1.973(4)	2.014(3)
M1−N2	2.104(2)	1.916(2)	1.908(4)	1.934(4)	1.970(3)
M1−N3	2.140(2)	1.915(2)	1.920(4)	1.953(4)	2.004(3)
M1−N4	2.125(2)	1.910(2)	1.941(4)	1.959(4)	1.988(3)
M2−N5	2.155(2)		1.932(3)	1.973(4)	2.036(2)
M2−N6	2.121(2)		1.946(3)	1.955(4)	2.012(3)
M2−N7	2.135(2)		1.925(3)	1.957(4)	2.003(3)
M2−N8	2.079(2)		1.906(4)	1.938(4)	1.980(3)
M1−O1	2.009(2)	1.867(2)	1.902(3)	1.929(3)	1.940(2)
M1−O2	2.083(2)	1.869(2)	1.900(3)	1.929(3)	1.960(2)
M2−O3	2.065(2)		1.887(3)	1.933(3)	1.976(2)
M2−O4	2.022(2)		1.883(3)	1.928(3)	1.944(2)
M−L_{av}	2.100(1)	1.903(1)	1.916(1)	1.947(1)	1.987(1)
C1−O1	1.277(3)	1.324(3)	1.285(5)	1.275(5)	1.280(3)
C2−O2	1.261(3)	1.315(3)	1.261(5)	1.269(5)	1.272(3)
C4−O3	1.262(3)		1.296(5)	1.269(5)	1.266(3)
C5−O4	1.265(3)		1.291(5)	1.273(5)	1.272(3)
C1−C2	1.540(3)	1.464(3)	1.512(6)	1.519(6)	1.518(3)
C2−C3	1.413(3)	1.401(4)	1.437(6)	1.395(6)	1.390(4)
C3−C4	1.397(3)	1.405(3)	1.381(6)	1.390(6)	1.400(4)
C4−C5	1.554(3)		1.526(5)	1.525(5)	1.530(3)
C5−C6	1.407(3)		1.400(6)	1.403(5)	1.400(4)
C6−C1	1.401(3)		1.374(6)	1.394(5)	1.404(4)
O···O bite	2.572(1)	2.551(3)	2.524(3)	2.508(3)	2.518(2)

[a] 208(2) K.[6] [b] 298(2) K.[6]

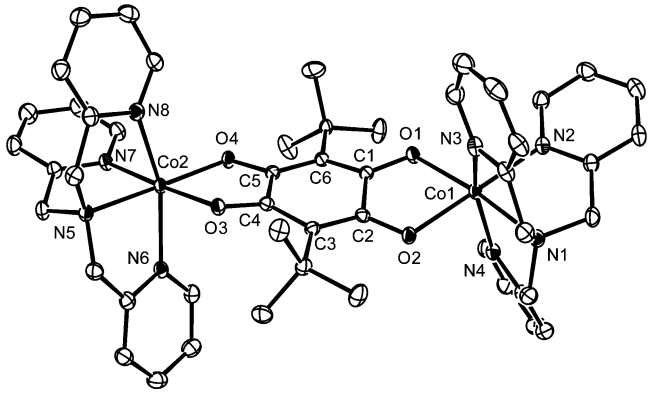

Figure 1. Structure of the $[(TPyA)Co^{II}(DBQ^{2-})Co^{II}(TPyA)]^{2+}$ ($\mathbf{1}^{2+}$). The atoms are represented by 40% probable thermal ellipsoids. This atom labeling diagram of the cations is the same for $\mathbf{1}^{n+}$ (n = 2, 3, 4) and $\mathbf{2}^{2+}$. H atoms, solvent, and $[BF_4]^-$ are omitted for clarity.

for the same dinuclear structure, and also shows the expected weak antiferromagnetic coupling (vide infra).

Structures. The crystal structures of dinuclear complexes [$\mathbf{1}^{n+}$ (n = 2, 3, 4), $\mathbf{2}^{2+}$] were determined by X-ray crystallography at low temperature; the crystallographic data are summarized in Table 1, and key bond distances are listed in Table 2. All complexes contain isostructural dimeric $[(TPyA)M(DBQ)M(TPyA)]^{n+}$ (M = Co, Fe; n = 2, 3, 4) cations with a tetradentate TPyA ligand. The representative ORTEP structure of the $\mathbf{1}^{2+}$ cation is shown in Figure 1. The cations in the crystal structures of $\mathbf{1}^{2+}$, $\mathbf{1}^{3+}$, and $\mathbf{1}^{4+}$, including $\mathbf{2}^{2+}$, are very similar and are not shown (see Supporting Information CIF files), and all cations have the identical atom labeling for easy comparison in Table 2. The oxidation states of the M^{n+} as well as change on the bridging DBQ^{n-} were elucidated from the observed bond distances and verified from magnetic and spectroscopic studies.

$\mathbf{1}^{2+}$·MeOH. The average Co−N_{TPyA} and Co−O_{DBQ} bond distances are 2.126(1) and 2.045(1) Å, respectively, and are characteristic of Co(II) ion.[13] The average C1−C2/C4−C5 and C−O bond distances of DBQ are 1.547(2) and 1.266(2) Å, respectively, and are characteristic of DBQ^{2-}.[6] The shortest intradimer Co···Co separation is 7.820(1) Å, which is 5.3% less than the shortest interdimer Co···Co separation of 8.254(1) Å. The pyridyl groups of $\mathbf{1}^{2+}$ are involved in extensive $\pi-\pi$ stacking interactions, with C−H···π interactions and offset face-to-face $\pi-\pi$ interactions.[14] Between the dimers, the pyridine ring involving N3 and N6 (x, $-y+0.5$, $z+0.5$) and the benzene rings of DBQ^{2-} (x, $-y+0.5$, $z+0.5$ and x, y, z) are $\pi-\pi$ stacked with the herringbone structure: H··· centroid, 2.59 and 2.82 Å; ∠C−H−centroid, 157 and 156°; centroid···centroid, 4.82 and 5.04 Å; and dihedral angle between the rings, 65 and 62°. Additionally, the pyridine group involving N3 located in a dimer undergoes the offset $\pi-\pi$ interaction with the pyridine group involving N6 (x, $-y+0.5$, $z+0.5$), which is positioned at the neighboring dimer. The interplanar separation of the pyridine rings is 3.04−3.61 Å (centroid···centroid, 3.98 Å) and the dihedral angle between the ring planes are 13.8°. Due to these interdimer offset face-to-face $\pi-\pi$ and herringbone interactions, $\mathbf{1}^{2+}$ forms a 1-D network (Figure 2a).

$\mathbf{1}^{3+}$·2MeCN. The average Co−N_{TPyA} and Co−O_{DBQ} bond distances are 1.921(1) and 1.868(1) Å, respectively. These are very short with respect to Co(II), and are characteristic of Co(III) ion.[5,13] The C1−C2 and average C−O bond distances are 1.464(3) and 1.320(2) Å, respectively. The former is significantly shorter and the latter significantly lengthened with respect to DBQ^{2-}, and are characteristic of $DBQ^{\bullet 3-}$.[3,5,6] The shortest intradimer Co···Co separation is 7.488(2) Å, which is 13% less than the shortest interdimer Co···Co separation of 8.580(1) Å. The pyridyl groups of $\mathbf{1}^{3+}$ are involved in extensive $\pi-\pi$ stacking interactions, with C−H···π interactions.[14] Between the dimers, the pyridine ring involving N2 and the benzene ring of $DBQ^{\bullet 3-}$ ($-x+0.5$, $y-0.5$, $-z+1.5$) are $\pi-\pi$ stacked with the herringbone structure: H···centroid, 2.99 Å; ∠C−H−centroid, 135°; centroid···centroid, 4.91 Å; and dihedral angle between the rings, 83.7°. Due to the herringbone interactions, $\mathbf{1}^{3+}$ forms a 2-D network (Figure 2b).

$\mathbf{1}^{4+}$·3MeCN. The average Co−N_{TPyA} and Co−O_{DBQ} bond distances are 1.930(1) and 1.893(2) Å, respectively. These are also very short with respect to Co(II), and are characteristic of Co(III) ion.[5,13] The average C1−C2/C4−C5 and C−O bond distances of DBQ are 1.520(4) and 1.283(3) Å, respectively, and are characteristic of DBQ^{2-}.[6] The shortest intradimer Co···Co separation is 7.499(1) Å that is 20% less than the shortest interdimer Co···Co separation of 9.391(1) Å. No meaningful intermolecular interactions exist between the dimers due to the large separation of the dimers.

$\mathbf{2}^{2+}$. At 208 K, the average Fe−N_{TPyA} and Fe−O_{DBQ} bond distances are 1.955(1) and 1.930(2) Å, respectively, and are characteristic of Fe(II) ion.[15] The average C1−C2/C4−C5 and C−O bond distances of DBQ are 1.523(4) and 1.272(3) Å, respectively, and are characteristic of DBQ^{2-}.[6] The shortest intradimer Fe···Fe separation is 7.616(1) Å and it is 6.5% less

(13) (a) Xie, Y.-B.; Li, J.-R.; Zhang, C.; Bu, X.-H. *Cryst. Growth Des.* **2005**, *5*, 1743. (b) Hossain, M. J.; Yamasaki, M.; Mikuriya, M.; Kuribayashi, A.; Sakiyama, H. *Inorg. Chem.* **2002**, *41*, 4058. (c) Konar, S.; Mukherjee, P. S.; Drew, M. G. B.; Ribas, J.; Chaudhuri, N. R. *Inorg. Chem.* **2003**, *42*, 2545.

(14) (a) Desiraju, G. R. *Crystal Engineering: The Design of Organic Solids*; Elsevier: New York, 1989; Chapter 4. (b) Shetty, A. S.; Zhang, J.; Moore, J. S. *J. Am. Chem. Soc.* **1996**, *118*, 1019. (c) Jennings, W. B.; Farrell, B. M.; Malone, J. F. *Acc. Chem. Res.* **2001**, *34*, 885.

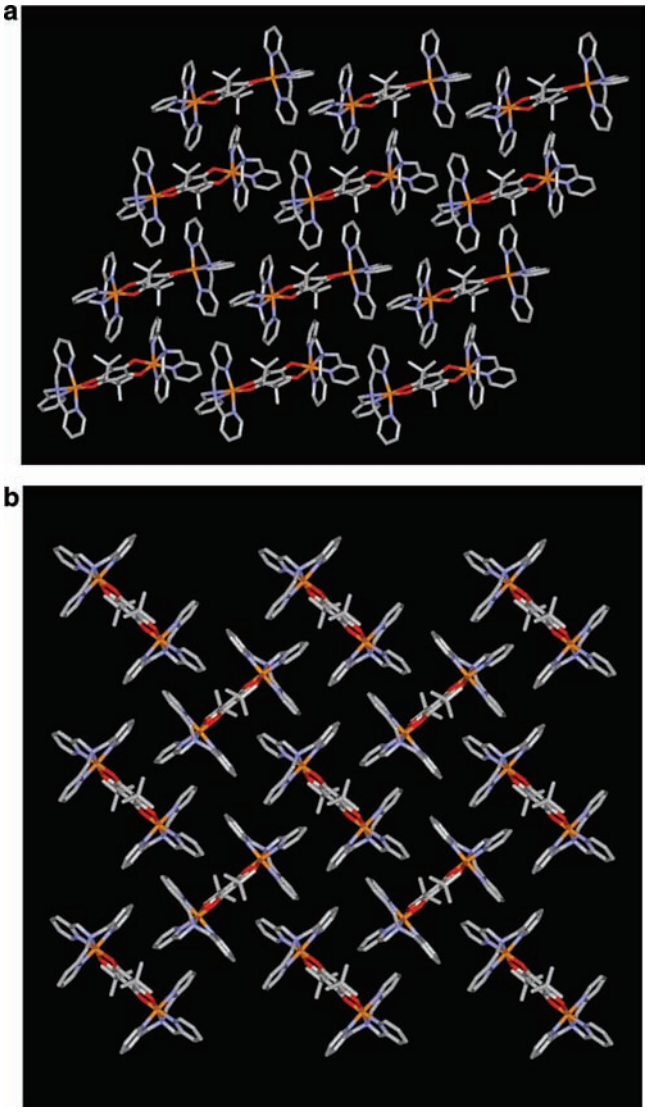

Figure 2. Perspective view of $\mathbf{1}^{2+}$ showing a 1-D polymer by C−H···π interactions and offset face-to-face $\pi-\pi$ interactions (a, top). The structure of $\mathbf{2}^{2+}$ is isomorphous to $\mathbf{1}^{2+}$. Extended 2-D structure of $\mathbf{1}^{3+}$ by C−H···π interactions (b, bottom).

than the shortest interdimer Fe···Fe separation of 8.149(1) Å. The pyridyl groups of $\mathbf{2}^{2+}$ are involved in extensive $\pi-\pi$ stacking interactions, with C−H···π interactions and offset face-to-face $\pi-\pi$ interactions.[14] Between the dimers, the pyridine rings involving N3 (x, $-y+0.5$, $z-0.5$) and N6 (x, $-y+0.5$, $z+0.5$) and the benzene ring of DBQ^{2-} are $\pi-\pi$ stacked with the herringbone structure: H···centroid, 2.73 and 2.64 Å; ∠C−H−centroid, 160 and 159°; centroid···centroid, 4.98 and 4.88 Å; and dihedral angle between the rings, 75.9 and 70.9°. Additionally, the pyridine group involving N3 located in a dimer undergoes the offset $\pi-\pi$ interaction with pyridine group involving N6 (x, $-y+0.5$, $z+0.5$), which is positioned at the neighboring dimer. The interplanar separation of the pyridine rings is ~3.49(5) Å (centroid···centroid, 3.92 Å) and the dihedral angle between the pyridine ring planes are 2.24°. Due to these interdimer offset face-to-face $\pi-\pi$ and herringbone interactions, $\mathbf{2}^{2+}$ forms a 1-D network (Figure 2a).

At 298 K, the average Fe−N_{TPyA} and Fe−O_{DBQ} bond distances for $\mathbf{2}^{2+}$ are 2.006(1) and 1.955(1) Å, respectively, and are again characteristic of Fe(II) ion.[15] The average C1−C2/C4−C5 and C−O bond distances of DBQ are 1.524(2) and 1.273(2) Å, respectively, and are characteristic of DBQ^{2-}.[6] The shortest intradimer Fe···Fe separation is 7.663(1) Å and it is 7% less than the shortest interdimer Fe···Fe separation of 8.251(1) Å. The pyridyl groups of $\mathbf{2}^{2+}$ are involved in extensive $\pi-\pi$ stacking interactions, with C−H···π interactions and offset face-to-face $\pi-\pi$ interactions.[14] Between the dimers, the pyridine rings involving N3 (x, $-y+0.5$, $z-0.5$) and N6 (x, $-y+0.5$, $z+0.5$) and the benzene ring of DBQ^{2-} are $\pi-\pi$ stacked with the herringbone structure: H···centroid, 2.76 and 2.68 Å; ∠C−H−centroid, 164 and 162°; centroid···centroid, 5.00 and 4.91 Å; and dihedral angle between the rings, 73.6 and 70.6°. Additionally, the pyridine group involving N3 located in a dimer undergoes the offset $\pi-\pi$ interaction with pyridine group involving N6 (x, $-y+0.5$, $z+0.5$), which is positioned at the neighboring dimer. The interplanar separation of the pyridine rings is ~3.56(5) Å (centroid···centroid, 3.99 Å) and the dihedral angle between the pyridine ring planes are 1.82°. Due to these interdimer offset face-to-face $\pi-\pi$ and herringbone interactions, $\mathbf{2}^{2+}$ forms a 1-D network (Figure 2a).

Magnetic Properties. Variable-temperature 2 to 300 or 380 K magnetic susceptibility, χ, measurements on polycrystalline samples of $\mathbf{1}^{n+}$ (n = 2, 3, 4), $\mathbf{2}^{n+}$ (n = 2, 3), and $\mathbf{3}^{2+}$ were studied. $\mathbf{1}^{4+}$ is diamagnetic between 2 and 300 K. Complex $\mathbf{1}^{2+}$ has a room-temperature effective moment, μ_{eff} [$=(8\chi T)^{1/2}$], of 6.68 μ_B/Co_2. This value is higher than the expected spin-only value of 5.48 μ_B indicative of a large spin−orbit coupling of Co(II) ions.[16] $\mu_{eff}(T)$ decreases slightly with decreasing temperature to 5.82 μ_B at 40 K, and then followed by a rapid decrease to 2.59 μ_B at 3 K, (Figure 3), indicating a very weak antiferromagnetic interaction within the Co(DBQ)Co unit. An analytical expression, eq 1 ($H=-2J\mathbf{S}_1\cdot\mathbf{S}_2$), for a coupled S = 3/2 dimer was fit $\chi(T)$ for $\mathbf{1}^{2+}$. The best fit had J/k_B of −3.20 K (−2.22 cm^{-1}), g = 2.44, θ = 0 K, and TIP = 400 × 10^{-6} emu/mol. The weak interaction can be attributed to a long intradimer distance between the Co(II) ions (7.820 Å). Hence, $\mathbf{1}^{2+}$ possesses $Co^{II}(DBQ^{2-})Co^{II}$.

$$\chi=[Ng^2\mu_B{}^2/k_B(T-\theta)]\{[2\exp(2J/k_BT)+10\exp(6J/k_BT)+28\exp(12J/k_BT)]/[1+3\exp(2J/k_BT)+5\exp(6J/k_BT)+7\exp(12J/k_BT)]\}+\mathrm{TIP} \quad (1)$$

The $\mu_{eff}(T)$ for $\mathbf{1}^{3+}$ is shown in Figure 3, and at 380 K its effective moment is 2.53 μ_B/Co_2. This value is between low spin S = 1/2 1.73 μ_B and high spin S = 3/2 3.87 μ_B spin-only expectations for Co(II). $\mu_{eff}(T)$ decreases with decreasing temperature until it reaches a plateau at ca. 300 K (1.75 μ_B). Below 300 K, $\mu_{eff}(T)$ is nearly constant until 5 K [μ_{eff} = 1.74(2) μ_B], indicating that the μ_{eff} values are consistent with the S = 1/2, and the data can be fit to the Curie−Weiss expression, $\chi \propto (T-\theta)^{-1}$ + TIP, with θ = −0.1 K, g = 2.005 as observed from the EPR spectrum (vide infra), and a TIP of 60 × 10^{-6}

(15) (a) Grunert, C. M.; Schweifer, J.; Weinberger, P.; Linert, W.; Mereiter, K.; Hilscher, G.; Müller, M.; Wiesinger, G.; van Koningsbruggen, P. J. *Inorg. Chem.* **2004**, *43*, 155. (b) Real, A.; Zarembowitch, J.; Kahn, O.; Solans, X. *Inorg. Chem.* **1987**, *26*, 2939. (c) Vos, G.; de Graaff, R. A. G.; Haasnoot, J. G.; van der Kraan, A. M.; de Vaal, P.; Reedijk, J. *Inorg. Chem.* **1984**, *23*, 2905. (d) Hagen, K. S. *Inorg. Chem.* **2000**, *39*, 5867.

(16) (a) Duggan, D. M.; Hendrickson, D. N. *Inorg. Chem.* **1975**, *14*, 1944. (b) Brewer, G.; Sinn, E. *Inorg. Chem.* **1985**, *24*, 4580. (c) Tandon, S. S.; Thompson, L. K.; Bridson, J. N.; Dewan, J. C. *Inorg. Chem.* **1994**, *33*, 54. (d) Glerup, J.; Goodson, P. A.; Hodgson, D. J.; Michelsen, K. *Inorg. Chem.* **1995**, *34*, 6255.

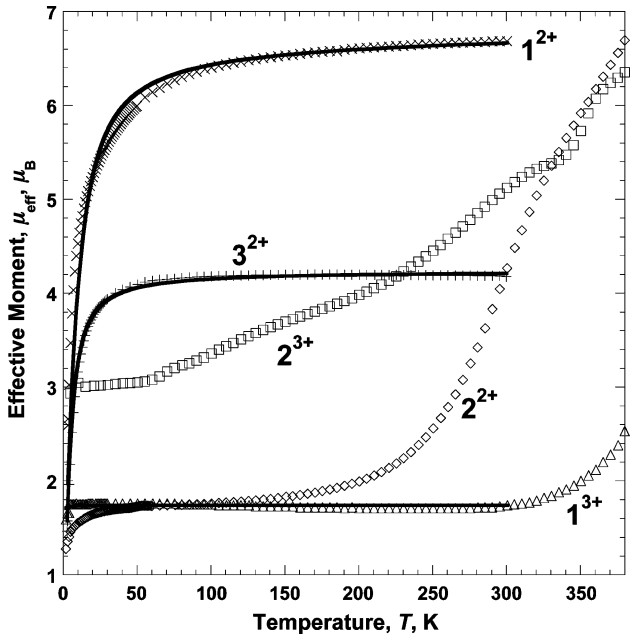

Figure 3. $\mu_{eff}(T)$ for $\mathbf{1}^{n+}$ [n = 2 (×), 3 (Δ)], $\mathbf{2}^{n+}$ [n = 2 (◇), 3 (□)], and $\mathbf{3}^{2+}$ (+). The solid lines are the best-fit curves to eqs 1−2, as discussed in the text.

emu/mol. This is in accord with the $[(TPyA)Co^{III}(DBQ^{\bullet 3-})Co^{III}(TPyA)]^{3+}$ electronic structure, and not S = 3/2 $[(TPyA)Co^{II}(DBQ^{2-})Co^{III}(TPyA)]^{3+}$. However, μ_{eff}(380 K) is higher than that of pure $[(TPyA)Co^{III}(DBQ^{\bullet 3-})Co^{III}(TPyA)]^{3+}$ and lower than $[(TPyA)Co^{II}(DBQ^{2-})Co^{III}(TPyA)]^{3+}$, i.e., above room temperature, based on the magnetic data, $\mathbf{1}^{3+}$ and its valence tautomerized species coexist in the solid state. Note that the substituents of bridged ligand (DBQ^{2-}) induce spin crossover, as $\mathbf{1}^{3+}$ displays spin crossover behavior due to the *t*-butyl groups in contrast to $[(TPyA)Co^{III}(CA^{\bullet 3-})Co^{III}(TPyA)](BF_4)_3$.[5] The spin crossover behavior is reproducible, but thermal hysteresis was not observed. This is in comparison to [(TPyA)Co(DHBQ)Co(TPyA)]$^{3+}$ (DHBQ = 1,4-dihydroxybenzoquinonate), which exhibits a thermal hysteresis due to intermolecular $\pi-\pi$ interactions.[3b] $\mathbf{1}^{3+}$ also has intermolecular $\pi-\pi$ interaction, but hysteresis was not observed. Furthermore, the X-band EPR spectrum of $\mathbf{1}^{3+}$ in MeCN solution at room temperature is shown an isotropic signal at g = 2.005. This EPR signal is consistent with a substantial organic radical character, but inconsistent with Co(II). Hence, $\mathbf{1}^{3+}$ is formulated as $[(TPyA)Co^{III}(DBQ^{\bullet 3-})Co^{III}(TPyA)]^{3+}$, and above room temperature it partially converts into its valence tautomeric isomer $[(TPyA)Co^{III}(DBQ^{2-})Co^{II}(TPyA)]^{3+}$, and is best described as a mixture of $[(TPyA)Co^{III}(DBQ^{\bullet 3-})Co^{III}(TPyA)]^{3+}$ and $[(TPyA)Co^{III}(DBQ^{2-})Co^{II}(TPyA)]^{3+}$.

The μ_{eff} for $\mathbf{2}^{2+}$ at 380 K is 6.69 μ_B/Fe_2. This is slightly lower than the expected spin-only value of 6.93 μ_B, and indicates that the magnetic spin states at 380 K do not fully recovered to high-spin Fe(II) ions.[17] $\mu_{eff}(T)$ decreases with decreasing temperature until it reaches a plateau at ca. 200 K (1.99 μ_B). Below 200 K, $\mu_{eff}(T)$ is nearly constant until 30 K, and exhibit a small residual amount (3.4%, g = 2.0) of high-spin Fe(II) ions at 2 K. Thermal hysteresis, however, was not observed. This is in comparison to $[(TPyA)Co(DHBQ)Co(TPyA)]^{3+}$, which exhibits a thermal hysteresis that is attributed to intermolecular $\pi-\pi$ interactions.[3b] Remarkably, however, $\mathbf{2}^{2+}$ shows a spin transition at ~300 K, as the moment abruptly increases. This behavior is anomalous as most metal complexes with DHBQ and CA exhibit weak antiferromagnetic coupling between paramagnetic species due to the long intradimer separation (~8.0 Å) and do not exhibit spin crossover. Thus, the substituents of bridged ligand (DBQ^{2-}) are very important to induce a spin crossover, in which $\mathbf{2}^{2+}$ exhibits spin crossover due to the electron donating *t*-butyl groups.

Between 2 and 50 K the $\mu_{eff}(T)$ of $\mathbf{2}^{3+}$ is 3.00(5) μ_B, indicative of the low-spin Fe^{III}; hence, it is formulated as $[(TPyA)Fe^{III}(DBQ^{\bullet 3-})Fe^{III}(TPyA)]^{3+}$, as it is in accord with the expected spin-only value (3.00 μ_B) in (1/2, 1/2, 1/2) spin system. $\mu_{eff}(T)$ increases continuously with increasing temperature to 5.38 μ_B at 380 K. Thus, the low spin Fe(III) dimer exhibits spin crossover to high-spin Fe(III) at higher temperature, i.e., (1/2, 1/2, 1/2) → (5/2, 1/2, 5/2). Below 330 K, the magnetic data are reproducible. However, when the magnetic data are taken again upon decreasing the temperature from 380 to 20 K, $\mu_{eff}(T)$ is not reproduced. This indicates that $\mathbf{2}^{3+}$ undergoes a phase change at ~330 K, due to thermal treatment. Thus, $\mu_{eff}(T)$ increases sharply at about 330 K in a staircase fashion. Furthermore, the magnetic moment at 380 K did not completely reach the value expected for high spin Fe(III), i.e., 8.54 μ_B/Fe_2. The IR spectra of $\mathbf{2}^{2+}$ and $\mathbf{2}^{3+}$ have significant differences indicating that the bridging ligand, not the metal ion, has different environments, i.e., different oxidation states. That is, DBQ^{2-} and $DBQ^{\bullet 3-}$ have different electronic structures, as verified by $[(TPyA)Fe_{ls}^{II}(DBQ^{2-})Fe_{ls}^{II}(TPyA)]^{2+}$, $[(TPyA)Fe_{hs}^{II}(DBQ^{2-})Fe_{hs}^{II}(TPyA)]^{2+}$, $[(TPyA)Co^{II}(DBQ^{2-})Co^{II}(TPyA)]^{2+}$, and $[(TPyA)Co^{III}(DBQ^{\bullet 3-})Co^{III}(TPyA)]^{3+}$, etc. Hence, based on the IR spectra $\mathbf{2}^{3+}$ is best described as $[(TPyA)Fe_{ls}^{III}(DBQ^{\bullet 3-})Fe_{ls}^{III}(TPyA)]^{3+}$ at low temperature. However, as the temperature increases, the $[(TPyA)Fe_{hs}^{III}(DBQ^{2-})Fe_{hs}^{II}(TPyA)]^{3+}$ excited-state becomes populated, and both $[(TPyA)Fe_{hs}^{III}(DBQ^{\bullet 3-})Fe_{hs}^{III}(TPyA)]^{3+}$ and $[(TPyA)Fe_{hs}^{III}(DBQ^{2-})Fe_{hs}^{II}(TPyA)]^{3+}$ are present in accord with the observed complex magnetic data.

The room temperature μ_{eff} of $\mathbf{3}^{2+}$ is 4.18 μ_B/Ni_2. This value exceeds the 4.00 μ_B expected for independent g = 2, S = 1, and this is attributed to a high effective Landé g value, i.e., g_{eff} = 2.13, that is typical of Ni(II) ions.[18] $\mu_{eff}(T)$ decreases slightly with decreasing temperature to 3.94 μ_B at 30 K, and thus, followed by a rapid decrease to 1.46 μ_B at 3 K (Figure 3), indicating a very weak antiferromagnetic interaction within the $Ni^{II}(DBQ^{2-})Ni^{II}$ unit. An analytical expression, eq 2 ($H = -2J\mathbf{S}_1\cdot\mathbf{S}_2$), for a coupled S = 1 dimer The $\chi(T)$ was fit to $\mathbf{3}^{2+}$. The best fit had J/k_B of −3.22 K (−2.24 cm^{-1}) and g = 2.13. This weak antiferromagnetic interaction can be attributed to a long intradimer distance between the Ni(II) ions.

$$\chi = [Ng^2\mu_B{}^2/k_B(T-\theta)]\{[2\exp(2J/k_BT) + 10\exp(6J/k_BT)]/[1+3\exp(2J/k_BT)+5\exp(6J/k_BT)]\} \quad (2)$$

Electrochemistry. The CV of $\mathbf{1}^{2+}$ in MeCN reveals three reversible one-electron transfer waves at $E_{1/2}$ (vs SCE) = 0.329, 0.007, and −1.121 V, and a fourth wave at −1.741 V that exhibits a slight chemical irreversibility (Figure 4). The two waves at positive potentials correspond to two successive one-electron oxidations ($\mathbf{1}^{2+}/\mathbf{1}^{3+}$ and $\mathbf{1}^{3+}/\mathbf{1}^{4+}$), while the waves at negative potentials correspond to two successive one-electron

(17) Assuming spin-only, g = 2 for high-spin Fe(II), 93% is recovered, and is an upper limit.

(18) Boudreaux, E. A.; Mulay, L. N. *Theory and Applications of Molecular Paramagnetism*; Wiley-Interscience: New York, 1976; p 226.

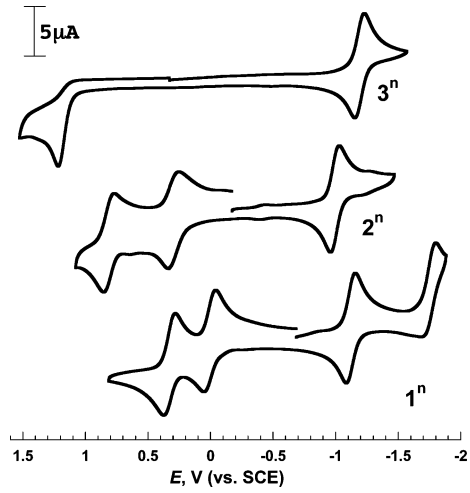

Figure 4. Cyclic voltammetry of $\mathbf{1}^{2+}$ (bottom), $\mathbf{2}^{2+}$ (middle), and $\mathbf{3}^{2+}$ (top) at 20 °C in MeCN solution, respectively, 0.1 M $[N(n\text{-}Bu)_4]BF_4$ supporting electrolyte; platinum working electrode; scan rate 100 mV/s.

reductions ($\mathbf{1}^{2+}/\mathbf{1}^{+}$ and $\mathbf{1}^{+}/\mathbf{1}^{\circ}$) of $\mathbf{1}^{2+}$, with the irreversibility of the wave at −1.741 V indicating that $\mathbf{1}^{\circ}$ is unstable on the voltammetric time scales used (100 mV/s). These potentials suggest that $\mathbf{1}^{n+}$ ($n = 3, 4$) can be isolated from oxidation with $FcBF_4$ and $ThianBF_4$, respectively, consistent with the formation of $\mathbf{1}^{3+}$ and $\mathbf{1}^{4+}$ using oxidants (vide supra). The mono-oxidation potential of $\mathbf{1}^{2+}$ (0.007 V) is similar to that of $[(TPyA)Co^{II}(CA^{2-})Co^{II}(TPyA)]^{2+}$ (0.094 V); however, the second oxidation and monoreduction potentials of $\mathbf{1}^{2+}$ (0.329 and −1.121 V) are more negative than those of $[(TPyA)Co^{II}(CA^{2-})Co^{II}(TPyA)]^{2+}$ (0.619 and −0.619 V, respectively). Hence, the two-electron oxidation of $\mathbf{1}^{2+}$ occurs more easily than $[(TPyA)Co^{II}(CA^{2-})Co^{II}(TPyA)]^{2+}$, while the first and second reductions of $\mathbf{1}^{2+}$ are more difficult than for $[(TPyA)Co^{II}(CA^{2-})Co^{II}(TPyA)]^{2+}$. This is in accord with the *t*-Bu group being a stronger electron donating group with respect to Cl.

The CV of $\mathbf{2}^{2+}$ shows three reversible one-electron transfer waves at $E_{1/2}$ (vs SCE) = 0.802, 0.281, and −1.007 V (Figure 4). The former two processes correspond to two successive one-electron oxidations ($\mathbf{2}^{2+}/\mathbf{2}^{3+}$ and $\mathbf{2}^{3+}/\mathbf{2}^{4+}$), and the latter to a one-electron reduction ($\mathbf{2}^{2+}/\mathbf{2}^{+}$). The CV of $\mathbf{3}^{2+}$ exhibits a reversible one-electron reduction ($\mathbf{3}^{2+}/\mathbf{3}^{+}$) at −1.191 V and a chemically irreversible one-electron oxidation ($\mathbf{3}^{2+}/\mathbf{3}^{3+}$) at 1.218 V that correspond to ligand and/or metal-centered processes (Figure 4). Thus, complexes $\mathbf{2}^{2+}$ and $\mathbf{3}^{2+}$ can be chemically oxidized and/or reduced.

As concluded from the structural, spectroscopic and magnetic data discussed above, valence ambiguous $\mathbf{1}^{3+}$ contains $DBQ^{\bullet 3-}$. That is, the one-electron oxidation of $\mathbf{1}^{2+}$ results in reduction of the bridging DBQ^{2-} ligand, and oxidation of both Co^{II} centers. This is in accord with the previously reported one-electron oxidation of $[(TPyA)Co^{II}(CA^{2-})Co^{II}(TPyA)]^{2+}$ forming valence-ambiguous $[(TPyA)Co(CA)Co(TPyA)]^{3+}$ with the $[(TpyA)Co^{III}(CA^{\bullet 3-})Co^{III}(TPyA)]^{3+}$ electronic structure rather than the expected mixed-valent $[(TPyA)Co^{III}(CA^{2-})Co^{II}(TPyA)]^{3+}$ electronic structure.[5] This reaction is referred to as a RIET reaction because a redox event induces an internal electron transfer within the molecule.

The electrochemical *square scheme* that relates the four accessible oxidations states of $\mathbf{1}^{2+}$ based on combinations of the individual one-electron metal center ($Co^{II/III}$) and ligand [$DBQ^{2-/\bullet 3-}$ (and $CA^{2-/\bullet 3}$)] redox chemistries is depicted in

Scheme 1

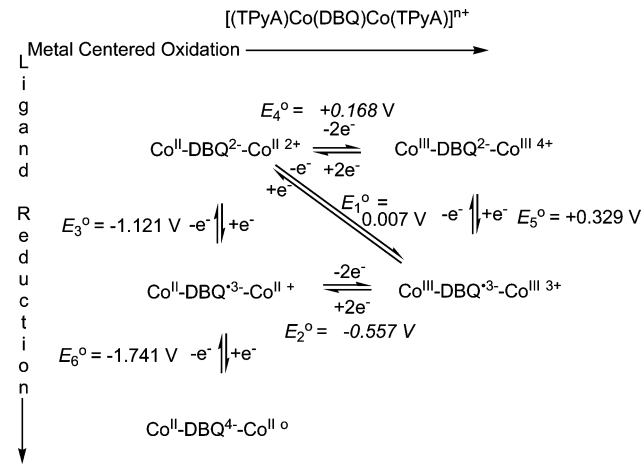

Scheme 1. Reactions shown horizontally correspond to changes in the oxidation state of the metal centers, while maintaining a constant redox state of the ligand. Conversely, reactions shown vertically correspond to changes in the oxidation state of the ligand, while maintaining a constant metal center oxidation state. In addition to the square scheme reactions, the reduction of $\mathbf{1}^{+}$ to $\mathbf{1}^{\circ}$ via ligand reduction ($E_6^{\circ} = -1.741$ V) is shown as a vertical reaction in the bottom left corner of Scheme 1.

The oxidation of $\mathbf{1}^{2+}$ to $\mathbf{1}^{3+}$ corresponds to *concurrent* Co^{II} oxidation/DBQ^{2-} reduction with a measured $E_1^{\circ} = 0.007$ V. The redox potentials for the ligand based oxidation of $\mathbf{1}^{3+}$ to $\mathbf{1}^{4+}$ ($E_5^{\circ} = 0.329$ V) and ligand-based reduction of $\mathbf{1}^{2+}$ to $\mathbf{1}^{+}$ ($E_3^{\circ} = -1.121$ V) are also determined from the experimental data (Figure 4). By combining redox reactions and using simple free energy relationships, the redox potentials for the 2-electron metal centered oxidation of $\mathbf{1}^{2+}$ to $\mathbf{1}^{4+}$ in either the presence of DBQ^{2-} or $DBQ^{\bullet 3-}$ can be readily computed, even though neither of these two processes is directly observable in the voltammetric data. For instance, addition of reaction 1 ($\mathbf{1}^{3+} + e^{-} = \mathbf{1}^{2+}$) and reaction 3 ($\mathbf{1}^{2+} + e^{-} = \mathbf{1}^{1+}$) yields reaction 2 ($\mathbf{1}^{3+} + 2\ e^{-} = \mathbf{1}^{+}$). The thermodynamic redox potential of reaction 2, E_2°, is computed as $[(n_1E_1^{\circ} + n_3E_3^{\circ})/n_2] = \{[(1)(0.007\text{ V}) + (1)(-1.121\text{ V})]/2\} = -0.557$ V (where n_i is the number of electrons transferred in the *i*th reaction). By a similar calculation, the thermodynamic redox potential of reaction 4 ($E_4^{\circ} = 0.168$ V) is obtained by combination of reactions 1 and 5.

The similarity of the redox chemistry of $[(TPyA)Co(CA)Co(TPyA)]^{2+}$ to $\mathbf{1}^{2+}$, and confirmation of $CA^{\bullet 3-}$ in the one-electron oxidation product of $[(TPyA)Co(CA)Co(TPyA)]^{2+}$,[5] suggests a square scheme for $[(TPyA)Co(CA)Co(TPyA)]^{2+}$, completely analogous to that of $\mathbf{1}^{2+}$.

Oxidation of $\mathbf{1}^{2+}$ to $\mathbf{1}^{3+}$ occurs by *concurrent* Co^{II} oxidation and DBQ^{2-} reduction and indicates that the formation of a bridging $DBQ^{\bullet 3-}$ is energetically stabilized by the higher valence Co^{III} metal centers. Equivalently, the formation of Co^{III} is stabilized by the presence of a reduced bridging ligand ($DBQ^{\bullet 3-}$). That is, the formation of $\mathbf{1}^{3+}$ may occur by reaction 4 followed by reaction 5 (an oxidative-reduction pathway), or by reaction 3 followed by reaction 2 (a reductive-oxidation pathway). Both mechanisms are energetically equivalent. While the mechanism of the multi electron transfer oxidation of $\mathbf{1}^{2+}$ to $\mathbf{1}^{3+}$ is unknown, the energy of stabilization for oxidizing the Co^{II} centers in the presence of $DBQ^{\bullet 3-}$ (reaction 2), relative to oxidizing the Co^{II} centers in the presence of DBQ^{2-} (also equivalent to the energy of stabilization for reducing the DBQ^{2-}

Scheme 2

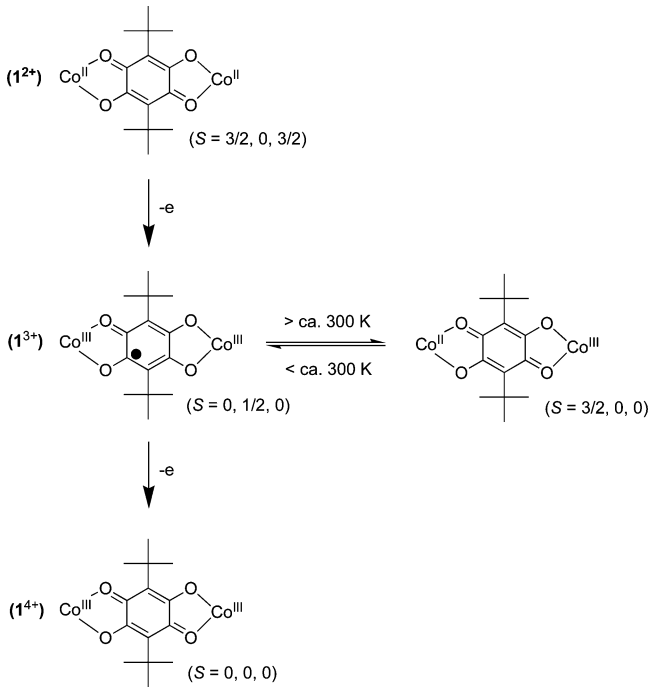

ligand in the presence of Co^{III}, relative to reducing the DBQ^{2-} ligand in the presence of Co^{II}), is computed from $n_4(E_4^\circ - E_2^\circ) = n_5(E_5^\circ - E_3^\circ)$ to be 1.45 eV (33.4 kcal/mol). The computed energy of stabilization for reducing the CA^{2-} analogue, $[(TPyA)Co(CA)Co(TPyA)]^{2+}$, is 1.24 eV (28.6 kcal/mol), using the previously reported voltammetric data.[5]

Conclusion

A series of six dinuclear compounds of $[(TPyA)M^m(DBQ)M^m(TPyA)]^{n+}$ (M = Co, Fe, Ni; m = II, III; n = 2, 3, 4) composition, i.e., $[(TPyA)M^{II}(DBQ^{2-})M^{II}(TPyA)]^{2+}$ [Co = ($\mathbf{1}^{2+}$), Fe = ($\mathbf{2}^{2+}$), Ni = ($\mathbf{3}^{2+}$)], $[(TPyA)M^{III}(DBQ^{\bullet 3-})M^{III}(TPyA)]^{3+}$ [Co = ($\mathbf{1}^{3+}$), Fe = ($\mathbf{2}^{3+}$)], and $[(TPyA)Co^{III}(DBQ^{2-})Co^{III}(TPyA)]^{4+}$($\mathbf{1}^{4+}$) have been prepared and characterized. The M ions in **1** and **2** display a distorted octahedral geometry by coordination with four nitrogens of a TPyA and two oxygens of a $DBQ^{2-/\bullet 3-}$. Due to the interdimer offset face-to-face $\pi-\pi$ and/or herringbone interactions, $\mathbf{1}^{2+}$, $\mathbf{1}^{3+}$, and $\mathbf{2}^{2+}$ show extended 1-D and/or 2-D supramolecular structures. Compound $\mathbf{1}^{3+}$ has the $DBQ^{\bullet 3-}$ trianion radical bridging ligand, and it occurs unexpectedly in valence ambiguous $\mathbf{1}^{3+}$. The existence of $DBQ^{\bullet 3-}$ in $\mathbf{1}^{3+}$ is characterized by structural, solid-state magnetic susceptibility and solution EPR spectroscopy. Valence ambiguous $\mathbf{1}^{3+}$ forms via a redox-induced electron transfer whereby the one-electron oxidation of the $[Co^{II}(DBQ^{2-})Co^{II}]^{2+}$ core forms $[Co^{III}(DBQ^{\bullet 3-})Co^{III}]^{3+}$, and the species is also shown spin crossover behavior over room temperature (Scheme 2). Co- and Ni-based $\mathbf{1}^{2+}$ and $\mathbf{3}^{2+}$ show weak antiferromagnetic interactions, while Fe-based $\mathbf{2}^{2+}$ exhibits strong spin crossover behavior around room temperature.

Acknowledgment. We appreciate the continued partial support by the Department of Energy Division of Material Science (Grant No. DE-FG03-93ER45504), U.S. National Science Foundation (Grant No. 0553573), and Army Research Office (Grant No. DAAD19-01-1-0562).

Supporting Information Available: X-ray crystallographic data in CIF format [CCDC no. 719173 ($\mathbf{1}^{2+}$), 719174 ($\mathbf{1}^{3+}$), 719175 ($\mathbf{1}^{4+}$), 662710 ($\mathbf{2}^{2+}$, at 208 K), 662711 ($\mathbf{2}^{2+}$, at 295 K)]. This material is available free of charge via the Internet at http://pubs.acs.org.

JA900909U